Journal of Electronic Research and Application, 2025, Volume 9, Issue 6
http://ojs.bbwpublisher.com/index.php/JERA
ISSN Online: 2208-3510
ISSN Print: 2208-3502

Design and Implementation of a 360° Panorama Imaging System Based on Motor-Driven Fisheye Camera

Yongsheng Sun, Xiaojuan Li, Guanjiang Liu, Yue Li, Huayang Zheng, Jianke Li*

Hebei University of Economics and Business, Shijiazhuang 050061, Hebei, China

**Author to whom correspondence should be addressed.*

Abstract: This paper designs and implements a single-camera 360° panoramic imaging system based on motor-driven fisheye rotation. The system utilizes a stepper motor for precise angular control, enabling the camera to rotate around its optical center to capture multi-view images, thereby avoiding the parallax and geometric mismatch problems inherent in traditional multi-camera configurations. To address the strong distortion characteristics of fisheye images, an equidistant projection model is adopted for distortion correction. On this basis, a brightness normalization method combining global linear brightness correction and local illumination compensation is proposed to enhance stitching consistency. By establishing a geometry model constrained by camera rotation and integrating cylindrical projection with cosine-weighted blending, the system achieves high-precision panoramic stitching and seamless visual transitions.

Keywords: Fisheye camera; Optical center alignment; Brightness normalization; Panoramic stitching

Online publication: December 16, 2025

1. Introduction

Panoramic image stitching technology has been widely applied in fields such as virtual reality (VR), 3D reconstruction, video surveillance, and autonomous driving [1]. Traditional panoramic imaging systems typically adopt multi-camera array structures, where multiple viewpoints are captured simultaneously to achieve panoramic reconstruction. However, such multi-camera configurations face significant challenges in maintaining optical-center consistency, exposure balance, and geometric calibration, while also incurring high hardware costs and complex installation requirements [2].

In contrast, feature-based stitching methods using handheld or moving cameras provide greater flexibility but tend to suffer from feature mismatches and visible seams under low-texture, variable-illumination, or motion-induced conditions due to the absence of stable extrinsic constraints [3,4].

To address these limitations, this study proposes a single-camera 360° panoramic acquisition system driven

by a stepper motor and equipped with a fisheye lens. The system enables automated multi-angle image capture by precisely rotating the camera around its optical center. Compared with conventional multi-camera schemes, the proposed design maintains a single optical center, thereby eliminating parallax errors inherent in multi-view stitching. To ensure imaging accuracy, an adjustable mounting structure is employed, allowing fine-tuning of the camera's position in three axes to align the optical center with the rotation axis. A chessboard-based calibration method is further used to estimate the camera intrinsic parameters and distortion coefficients, enabling high-precision geometric correction [5,6].

2. System design

As shown in **Figure 1**, the system consists of three main components: image acquisition, image stitching, and motor control. The modules collaborate via UART and Ethernet Port, enabling automated acquisition and processing of panoramic images.

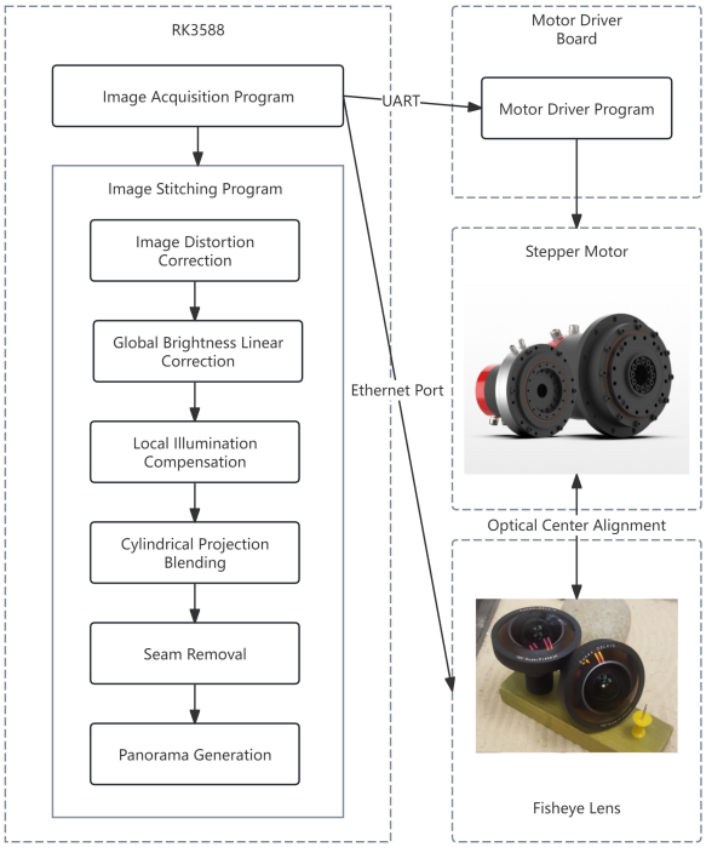

Figure 1. System architecture diagram.

2.1. Data acquisition

2.1.1. Motor structure and rotation control principle

The system employs a stepper motor as the rotational drive unit. Precise angular control is achieved via the motor driver module in conjunction with the main microcontroller. The motor is connected to the camera mount through a coupler, with the mount's center aligned along the system's rotation axis. Based on the full panorama coverage

and the camera's field of view (FOV), the rotation step is designed, typically set between 60° and 120° per step, ensuring sufficient overlap between adjacent images to facilitate subsequent stitching.

2.1.2. Camera calibration

To minimize stitching errors, the camera's optical center must be strictly aligned with the system's rotation axis. This system adopts an adjustable mount structure, equipped with sliding rails and threaded fine-tuning mechanisms, allowing precise adjustment in three directions to align the fisheye camera's optical center with the rotation axis.

The following demonstrates the calibration process and results. Before optical center calibration, the camera's optical center deviates from the rotation axis, causing noticeable relative motion between foreground and background objects when the camera rotates around the axis (**Figure 2**), manifested as significant parallax (**Figure 3**). During calibration, the camera's position is gradually adjusted along the X, Y, and Z axes to maximize the alignment of foreground and background edges before and after rotation. When the distance ratio between the camera and the foreground/background is 1:5, the relative displacement between them must not exceed 5 mm. Once the parallax falls below this threshold, the optical center calibration is considered complete (**Figure 4**).

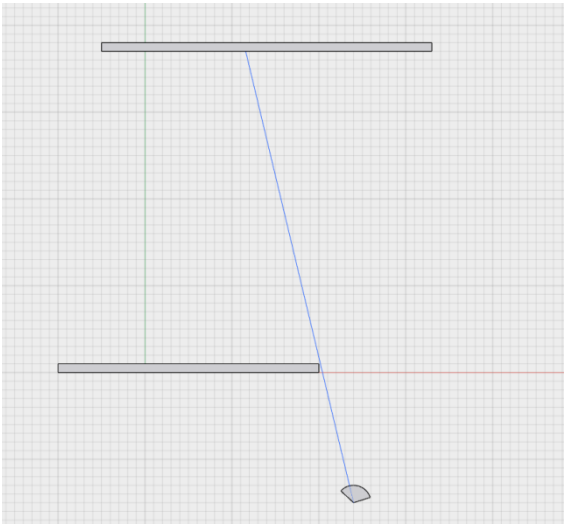

Figure 2. Optical center calibration method.

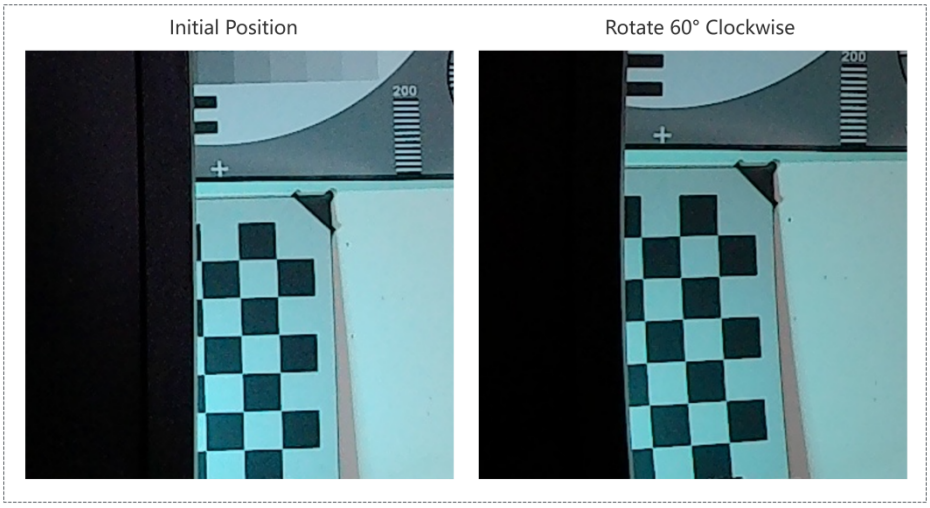

Figure 3. Before optical center calibration.

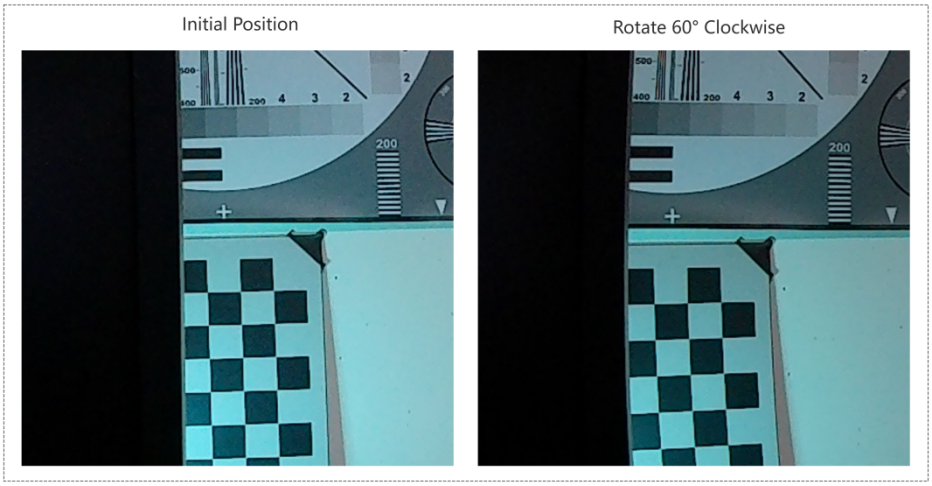

Figure 4. After optical center calibration.

During the calibration process, 50–60 images of a 12×9 chessboard taken from different angles were used. The intrinsic matrix K and distortion coefficients D were computed using the pinhole camera model. The intrinsic matrix takes the following form:

$$K = \begin{bmatrix} f_x & 0 & c_x \\ 0 & f_y & c_y \\ 0 & 0 & 1 \end{bmatrix} \tag{1}$$

Here, f_x and f_y are the focal lengths in pixels, and C_x and C_y are the coordinates of the principal point. The distortion model considers both radial and tangential distortions:

$$\begin{aligned} x_{corr} &= x\left(1 + k_1 r^2 + k_2 r^4 + k_3 r^6\right) + 2p_1 xy + p_2\left(r^2 + 2x^2\right) \\ y_{corr} &= y\left(1 + k_1 r^2 + k_2 r^4 + k_3 r^6\right) + p_1\left(r^2 + 2y^2\right) + 2p_2 xy \end{aligned} \tag{2}$$

Here, k_i and p_i are the radial and tangential distortion coefficients, respectively.

Through this calibration process, the system achieves a high degree of alignment between the optical center and the rotation axis, while simultaneously computing the camera intrinsic parameters. This ensures that all frames captured during rotational acquisition maintain consistent spatial projection and imaging parameters, providing precise constraints for subsequent geometric mapping and stitching fusion.

2.1.3. Synchronized acquisition control logic

The acquisition control is implemented by the main controller RK3588, which coordinates the synchronized operation of the motor and camera. The control logic is as follows:

(1) The main controller sends a rotation angle command to the motor driver board via the serial port;
(2) The motor driver board converts the command into stepper pulses to drive the motor;
(3) The motor rotates to the target angle and stops;
(4) The motor driver board returns a “completion” signal to the main controller;
(5) The main controller sends a trigger signal to the camera via the Ethernet port;
(6) After exposure and image storage, the camera returns a “completion” signal;

(7) Upon confirming the signal, the main controller proceeds to the next rotation cycle.

This logic prevents image blur caused by triggering the camera before the motor fully stops, ensuring that each captured image has precise and consistent positioning.

2.2. Image distortion correction

After the system acquires images from the fisheye camera, a preprocessing step is required to eliminate optical distortion. Fisheye lenses have an extremely wide field of view, but their imaging model differs from conventional lenses, often exhibiting significant radial distortion. In this work, a distortion correction method based on an equidistant projection model extended from the pinhole model is adopted [7]. The imaging relationship of the fisheye camera can be expressed as:

$$r = f \cdot \theta \tag{3}$$

Here, r is the radial distance from a point to the image center, f is the effective focal length, and θ is the angle between the incident ray and the optical axis.

During camera calibration, a set of feature point pairs is obtained from a calibration board with known dimensions. The intrinsic matrix K and distortion parameter vector $D = [k_1, k_2, k_3, k_4]$ are determined by minimizing the reprojection error. The relationship between image coordinates and normalized coordinates can be expressed as:

$$\begin{bmatrix} x_c \\ y_c \\ 1 \end{bmatrix} = K^{-1} \begin{bmatrix} u \\ v \\ 1 \end{bmatrix}, \quad \begin{cases} x' = x_c\left(1 + k_1 r^2 + k_2 r^4 + k_3 r^6 + k_4 r^8\right) \\ y' = y_c\left(1 + k_1 r^2 + k_2 r^4 + k_3 r^6 + k_4 r^8\right) \end{cases} \tag{4}$$

where (u,v) are the original pixel coordinates and (x',y') are the normalized coordinates after distortion correction.

The core of distortion correction is to remap all pixels to the ideal imaging plane so that the imaging optical center aligns with the geometric center, thereby reducing projection errors during the stitching process.

2.3. Image brightness normalization

After distortion correction, to further improve brightness consistency and seam smoothness in image stitching, this study adopts a brightness normalization algorithm combining global linear brightness correction with local illumination compensation. This method maintains overall exposure balance while suppressing local brightness variations caused by changes in ambient light.

2.3.1. Global linear brightness correction

Let the i-th image captured during rotation be $I_i(x,y)$. Its brightness is linearly adjusted using a global gain g_i and bias b_i, such that the brightness difference in the overlapping regions with adjacent images is minimized. For any pair of images i and j with overlapping regions, we have:

$$g_i I_i(p) + b_i \approx g_j I_j(p), \; p \in \omega_{ij} \tag{5}$$

Here, Ω_{ij} denotes the set of overlapping pixels between images i and j.

To obtain the optimal g_i and I_i, the following least-squares objective function is constructed:

$$E(g,b) = \sum_{(i,j)} \sum_{p \in \Omega_{ij}} \left(g_i I_i(p) + b_i - g_j I_j(p) \right)^2 + \gamma_g \sum_i (g_i - 1)^2 + \gamma_b \sum_i b_i^2 \quad (6)$$

Here, γ_g and γ_b are regularization coefficients used to constrain the range of brightness scaling and offset.

By fixing the parameters of a reference image as g_1=1 and b_1=0, the correction parameters for all images can be solved using linear least-squares. This process effectively eliminates overall brightness inconsistencies caused by camera exposure variations and illumination changes during motor rotation.

2.3.2. Local illumination compensation

Although global linear correction balances the overall brightness, local regions may still exhibit illumination gradients under different viewpoints. To further eliminate such low-frequency lighting differences, a low-frequency brightness field $S_i(x,y)$ is estimated for each image. This brightness field is extracted using bilateral filtering:

$$S_i(x) = \frac{1}{W(x)} \sum_{y \in N(x)} L_i(y) exp\left(-\frac{\|x-y\|^2}{2\sigma_s^2} \right) exp\left(-\frac{|L_i(x) - L_i(y)|^2}{2\sigma_r^2} \right) \quad (7)$$

Here, $L_i(x)$ is the luminance channel of the image, $N(x)$ denotes the pixel neighborhood, and σ_s and σ_r are the standard deviations for the spatial and intensity domains, respectively. $W(x)$ is the normalization factor.

The final pixel-level brightness correction model is expressed as:

$$\tilde{I}_i(x) = \frac{g_i I_i(x) + b_i}{S_i(x) + \varepsilon} \quad (8)$$

Here, ε is a small constant to prevent division by zero.

After this step, the overall image brightness is unified, and local illumination variations are suppressed, significantly improving the overall quality of subsequent stitching and fusion (**Figure 5**).

Figure 5. Comparison of images before and after brightness optimization.

2.4. Image stitching

To achieve seamless stitching of surround-view scenes, the system employs a high-precision image stitching algorithm based on rotational constraints between adjacent frames. Since the camera is rotated at fixed angles by the motor and its optical center remains fixed, undergoing only rotation around the vertical axis (Y-axis), a geometric transformation model between adjacent frames can be explicitly established. This reduces feature matching errors and improves stitching stability.

2.4.1. Establishing transformation between adjacent frames

Assume that the system captures a total of N images in the horizontal direction, and the motor rotates by an angle of:

$$\Delta\theta = \frac{360°}{N} \tag{9}$$

Let the camera pose of the i-th image be R_i. The rotational relationship between adjacent frames is given by:

$$R_{i+1} = R_i \cdot R_y(\Delta\theta) \tag{10}$$

$R_y(\Delta\theta)$ denotes the rotation matrix around the Y-axis by $\Delta\theta$:

$$R_y(\Delta\theta) = \begin{bmatrix} \cos\Delta\theta & 0 & \sin\Delta\theta \\ 0 & 1 & 0 \\ -\sin\Delta\theta & 0 & \cos\Delta\theta \end{bmatrix} \tag{11}$$

Since the optical center is fixed and the camera position does not change, translation estimation is unnecessary. Therefore, the registration process is significantly simplified, and spatial mapping between images can be completed using only rotational parameters.

2.4.2. Cylindrical projection and registration

Fisheye camera images exhibit strong radial distortion. To eliminate edge deformation and maintain visual continuity, all corrected images are projected onto a cylindrical coordinate system [8,9]. For each pixel (x,y) in a corrected image, its projection onto cylindrical coordinates is given by:

$$\begin{cases} \theta = \arctan\left(\frac{x}{f}\right) \\ h = \frac{y}{\sqrt{x^2 + f^2}} \cdot f \end{cases} \tag{12}$$

Here, f is the effective focal length, θ is the horizontal rotation angle, and h is the cylindrical height coordinate.

After projection, adjacent images are aligned to the same cylindrical coordinate system using the aforementioned rotation matrix $R_y(\Delta\theta)$ for overlap.

2.4.3. Seam removal and blending

Due to brightness differences and overlapping regions between frames, obvious seams may appear. To avoid this, the system employs a smooth weighted blending method (Feather Blending) to achieve seamless transitions. Let the weight function of the overlapping region be $w(x)$, defined as a cosine-based smooth weight:

$$w(x) = \frac{1}{2}\left[1 - \cos\left(\pi \frac{x - x_0}{d}\right)\right] \quad (13)$$

Here, x_0 is the start of the overlapping region, and d is the width of the overlap.

The pixel values of the final blended image are given by:

$$I_{blend}(x) = w(x)I_1(x) + [1 - w(x)]I_2(x) \quad (14)$$

This method achieves smooth brightness transitions at the boundaries, significantly reducing the perception of seams. As shown in **Figure 6** and **Figure 7**, **Figure 6** presents the stitching result before applying the feather blending, where noticeable brightness differences and seam artifacts are observed in the overlapping regions. **Figure 7** shows the result after blending, in which the overlapping regions exhibit significantly improved brightness continuity through cosine-weighted smoothing, rendering the seams almost imperceptible and achieving a more visually seamless panoramic image.

Figure 6. Before seam removal.

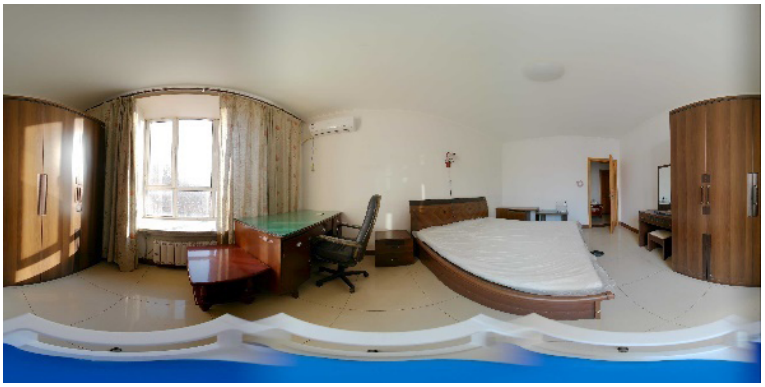

Figure 7. After seam removal.

2.4.4. Panorama generation

After all images are sequentially stitched according to the motor rotation angles, the system forms a continuous surround-view panorama in cylindrical coordinates. Finally, the panorama is unwrapped onto a 2D plane through inverse projection to generate the final 360° panoramic image, which can be used for subsequent display or environmental perception applications.

3. Experimental setup and results

3.1. Test environment

The experimental platform of the system consists of a motor control unit, a fisheye camera module, and the main control development board.

The motor is a stepper-type rotational drive with a step angle of 0.00225°, achieving precise angular positioning through microstepping control. The camera is mounted on a bracket above the motor, with its optical center calibrated to coincide with the rotation axis, ensuring that the images involve pure rotational motion only. The camera resolution is 5472 × 3648, with a field of view of 195° × 150.06°, and image acquisition is synchronized with the motor control signals via cable triggering. The main control board is equipped with an RK3588 processor, 4 GB RAM, and runs Ubuntu 20.04. All image processing and stitching algorithms are executed on this main control board.

The system was tested In two typical environments:

(1) Scene A (Indoor Laboratory): Stable lighting with dense object distribution, mainly used to verify registration accuracy;

(2) Scene B (Outdoor Landscape): Significant lighting variations with large brightness differences between sky and ground, used to evaluate brightness balancing and seamless fusion performance.

During acquisition, the motor rotates 120° per shot, capturing a total of 3 original images for panorama stitching.

3.2. Panorama stitching results and qualitative evaluation

After distortion correction and brightness normalization, images are registered and fused according to the cylindrical projection model. The stitching results show that the proposed system can generate high-precision panoramas under conditions of optical center-aligned rotational acquisition. The stitched images exhibit almost no visible seams at the edges, with continuous and natural color and brightness.

In the indoor experiment, the grayscale difference at the overlapping edges of the 3 images is less than 3%, indicating that the brightness correction and weighted blending algorithm effectively suppresses seams. In the outdoor experiment, the boundary between sky and ground maintains good geometric consistency without noticeable misalignment or stretching.

Figure 8, **Figure 9** and **Figure 10** show stitching results under different scenes, demonstrating that the system achieves consistent imaging under complex lighting conditions and large fields of view. Since the camera optical center is fixed, stitching errors mainly originate from minor rotational angle deviations and exposure differences, which are negligible after brightness normalization.

Figure 8. Indoor uniform lighting scene.

Figure 9. Outdoor scene.

Figure 10. Indoor low-light scene.

3.3. Performance evaluation

The overall system performance is evaluated using the seam smoothness and seamlessness metric as the key performance indicator [10]. The seam performance is assessed based on the brightness consistency in the blending regions. The seamlessness metric is defined as:

$$S = 1 - \frac{1}{N}\sum_{i=1}^{N}\frac{|I_L(i) - I_R(i)|}{255} \tag{15}$$

Here, $I_L(i)$ and $I_R(i)$ represent the pixel brightness values on the two sides of the seam, and N is the number of pixels in the seam region.

The closer S is to 1, the smoother the seam and the smaller the brightness difference. Based on the above metrics, the system's performance was evaluated on datasets from various scenarios. The resulting seamlessness index S, Mean Squared Error (MSE), and Visual Ratings are presented in **Table 1**.

Table 1. System performance evaluation results

Dataset scene	Dataset size	S	MSE	Visual rating
Uniform lighting scene	200	0.95	10.3	4.9
Outdoor natural light	200	0.93	14.2	4.7
Indoor low-light scene	200	0.94	12.6	4.8

The comprehensive experimental results indicate that the proposed depth-guided seamless blending algorithm

demonstrates high seam smoothness and visual consistency under various lighting and environmental conditions. The seamlessness metric consistently remains above 0.93, indicating natural brightness transitions in the blending regions with almost no visible seam artifacts. The mean squared error (MSE) is maintained at a low level, reflecting good brightness consistency. Additionally, subjective visual ratings generally exceed 4.7, confirming the stability and superiority of the algorithm in practical stitching scenarios. Overall, the system achieves the design goal of high-precision panorama stitching in terms of seam quality, exhibiting strong robustness and versatility, and future research will focus on the integration of the system with radar sensors [11].

4. Conclusion

This paper presents and implements a panoramic imaging system based on a motor-driven single fisheye camera. Through the collaborative optimization of hardware design and image processing algorithms, the system achieves high-precision, low-cost 360° panorama stitching. Experimental results demonstrate that the system can produce high-quality panoramic images with no obvious seams under various lighting and scene conditions. The employed cylindrical projection, brightness normalization, and cosine-based smooth blending methods effectively enhance visual continuity and imaging stability, validating the robustness and feasibility of this approach for single-camera rotational stitching. Future research will focus on the integration of the system with radar sensors. On one hand, panoramic images can be used to map colors onto radar point clouds, enabling visualization and semantic enhancement. On the other hand, radar-provided depth information can establish more accurate spatial geometric constraints to optimize depth consistency and boundary alignment in panoramic stitching. By leveraging the complementary strengths of vision and radar, the system's robustness under complex lighting and dynamic environments can be further improved, laying the foundation for multimodal environmental perception and 3D scene reconstruction. In summary, this study provides a complete system solution for high-precision single-camera panorama stitching, offering a new technical pathway for the development of low-cost visual perception systems.

Funding

Graduate Innovation Ability Training Program of the Hebei Provincial Department of Education, 2025 (Project No.: CXZZSS2025095)

Disclosure statement

The authors declare no conflict of interest.

References

[1] Ji F, 2025, Fast Image Stitching Algorithm for Intelligent Vehicle Panoramic Systems, thesis, Nanjing Forestry University.

[2] Liu X, Li H, 2024, Video Stitching Study of Rural Scenic Panoramic Identification System Based on Improved ORB Feature Detection. Automation and Instrumentation, 2024(10): 10–13.

[3] Li H, Wang L, Zhao T, et al. 2024, Local-Peak Scale-Invariant Feature Transform for Fast and Random Image Stitching. Sensors, 24(17): 5759.

[4] Ji Y, Ding P, Liu N, et al., 2024, Low-Illumination Image Stitching Method based on Improved SURF. *Laser & Optoelectronics Progress*, 61(18): 1837014.

[5] Qu K, Guo Z, Tang Y, et al. 2022, Zhang Zhengyou Calibration Algorithm Considering Object Coordinate Errors. Northwest Hydropower, 2022(6): 79–84.

[6] Lin L, Niu Q, Li Y, 2023, Optimized Camera Parameter Calibration Method Based on Chessboard Calibration Board. Computer Technology and Development, 33(12): 101–105.

[7] Hao J, Liu S, Zhang Y, 2023, A Stronger Stitching Algorithm for Fisheye Images Based on Deblurring and Registration, arXiv, https://doi.org/10.48550/arXiv.2307.11997

[8] Yang J, Liu J, Cui Y, et al. 2023, Research on Cylindrical-Based Aerial Panoramic Stitching Technology. Ship Electronic Engineering, 43(12): 62–64.

[9] Li X, Chen Z, Zhou L, 2022, Panoramic Image Generation Algorithm Based on Cylindrical Surface Mapping. Journal of Image and Graphics, 27(5): 1123–1132.

[10] Shin J, Rahim M, Yun K, 2018, Panoramic Image Stitching with Efficient Brightness Fusion Using RANSAC Algorithm. International Journal of Engineering and Technology, 7(3.34): 50–55.

[11] Wang T, Huang H, Cai Z, et al., 2024, 360° Panorama Stitching Method with Depth Information: Enhancing Image Quality and Stitching Accuracy, ISPRS Archives of the Photogrammetry. Remote Sensing and Spatial Information Sciences, XLVIII-4/W10-2024: 191–198.